First Principle Treatments on Site- and Size-Dependent Supermolecular Interactions and Nonlinear Optical Properties of Polymer of 2-Methyl-4-Nitroaniline

W.-D. Cheng,* D.-S. Wu, H. Zhang, X.-D. Li, D.-G. Chen, Y.-Z. Lang, Y.-C. Zhang, and Y.-J. Gong

Fujian Institute of Research on the Structure of Matter, Graduate School of the Chinese Academy of Sciences, State Key Laboratory of Structural Chemistry, Fuzhou, Fujian 350002, People's Republic of China

Received: November 10, 2003; In Final Form: May 19, 2004

We report the supermolecular interactions, electronic absorption spectra, and dynamic second-order nonlinear optical polarizabilities β of π-stacking (p-) and hydrogen-bonded (h-) dimers and a trimer in a 2-methyl-4-nitroaniline (MNA) crystal, using the TDB3LYP/3-21G+ coupled with the SOS methods. The calculated results show that the supermolecular interactions and second-order optical polarizabilities are smaller for dimers (p- and h-dimers) than the trimer in MNA crystal, which originates from size effect, and the h-dimer has smaller supermolecular interaction and larger second-order nonlinear optical response compared with that of the p-dimer, which originates from site effect in MNA crystal. The lowest absorption peak comes from the $\pi-\pi^*$ charge transfers within a MNA molecule for h-dimer, and between the two MNA molecules for the p-dimer in a MNA crystal. The calculated polarizability norm $||\beta||$ of trimer consisting of h- and p-arrangements is 42.0×10^{-30} cm^5 esu^{-1}, and the macroscopy susceptibility norm $||\chi||$ is 6.15×10^{-7} esu as compared with the experimental value $||\chi||$ of 9.06×10^{-7}esu in MNA crystal. The slipped cofacial arrangements of dimer (h-dimer) have larger contributions to the electronic absorption spectrum and nonlinear optical response of MNA crystal.

1. Introduction

It is well-known that 2-methyl-4-nitroaniline (MNA) crystal is an important nonlinear optical (NLO) material because it exhibits large phase matched second harmonic generation and figure of merit for NLO response.[1,2] Applications in the realm of short-pulse nonlinear optics,[3] electrooptic modulation,[4] and microcavity studies[5] have been reported for MNA crystal. Interest is aroused again for the investigations of this material due to the progress that has been made on oriented growth of MNA crystal on different substrates and to understanding of the orientation mechanisms.[6−9] Typical NLO organic molecules are generally made up of a conjugated π-electron system, with electron donor and acceptor groups attached at opposite sides of the molecule so as to induce charge transfers within the molecule and enhance the second-order NLO response. However, we need to consider how to hinder a centrosymmetric crystal packing and achieve a large second-order NLO response while the molecules stack and grow a bulk crystal material. Marks and co-workers found that the aggregate hyperpolarizability depends strongly on relative molecular orientations, and the slipped cofacial arrangement in molecular assemblies exhibit the largest hyperpolarizability based on the calculated results by the INDO combined with the sum-over states methods.[10] Accordingly, it is very interesting to understand packing mechanisms of molecular assemblies in a MNA crystal. It may give a clue to control of molecular arrangements in an organic crystal that has superior nonlinear optical properties.

In this work we will use the time-dependent B3LYP (TDB3LYP) method based on the 3-21G+ basis set to compute the supermolecular interaction strengths and electronic absorption spectra of monomer, p- and h-dimers, and trimer in a MNA crystal. Then, combined with the sum-over states (SOS) formula, we will calculate dynamic second-order polarizabilities of the studied species. We will also look into site- (p- and h-stacking) and size- (dimer and trimer) dependent nonlinear polarizabilities and the contributions of π-charge transfers and influence of MNA molecule assembling arrangements to the second-order optical susceptibility in MNA crystal, respectively.

2. Methods and Procedures

The electronic absorption spectra and supermolecular interactions are computed by using the time-dependent density functional theory (TDDFT) at the B3LYP/3-21G+ level[11−13] for the π-stacking and hydrogen-bonded dimers (p- and h-dimers) and trimer of MNA molecules. The calculations are performed with the Gaussian 98 program.[14] Becke' three parameter of Lee−Yang−Parr (B3LYP) hybrid function including exact exchange and correlation functions and the standard basis sets of 3-21G+ stored internally in the Gaussian 98 program are employed in the calculations. To describe an influence of basis set on hyperpolarizability β, we make the comparisons among the obtained values from the standard basis sets[14] of STO-3G, 3-21G, 3-21G+, and 6-31G+ in the calculations of monomer MNA molecule. It is found from Figure 1 that the obtained β values are close between the basis sets of 3-21G+ and 6-31G+ in the calculations using the ab initio CIS−SOS method. Accordingly, we employ the basis sets of 3-21G+ in the TDB3LYP calculations. The wave functions and energy eigenvalues of the excited states are determined by solving the time-dependent Kohn−Sham equation.[15,16] The SCF convergence criteria of the root-mean-square (rms) density matrix and the maximum density matrix are set at 10^{-8} and 10^{-6}, respectively, in all the electronic structure calculations.

* To whom correspondence should be addressed. E-mail: cwd@ms.fjirsm.ac.cn.

10.1021/jp0374096 CCC: $27.50
Published on Web 07/31/2004

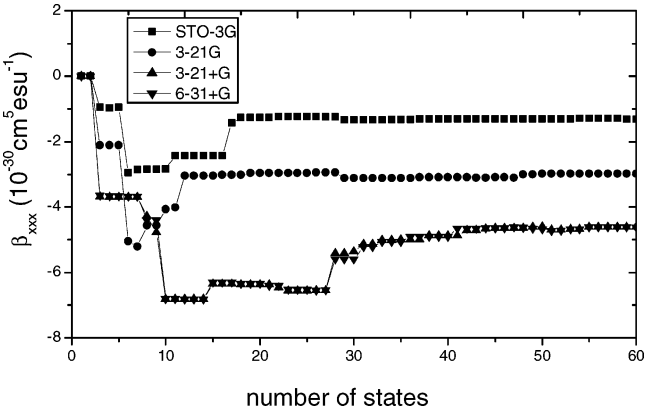

Figure 1. Convergent behavior of β_{xxx} with number of states considered in ab initio CIS−SOS calculations including different basis sets for single-MNA and double-MNA mlecules.

The range of molecular orbitals for correlation is from orbital 12 to 159 for the monomer MNA molecule, from orbital 23 to 318 for both the p- and h-dimers, and from orbital 34 to 477 for trimer of MNA supermolecules in the TDB3LYP calculations. The iterations of excited states are continued until the changes on energies of states are no more than 10^{-7} au between the iterations, and the convergence has been obtained in the all calculations.

NLO responses are calculated by standard time-dependent perturbation theory, and the Kohn−Sham Hamiltonian is uncoupled with the applied field. In the uncoupled schemes,[17,18] electronic excited states created by the perturbing field are treated as an infinite sum over unperturbed partical-hole states, and the dynamic first-order hyperpolarizabilities β_{ijk} are given as

$$\beta_{ijk}(\omega_3;\omega_1,\omega_2) = 1/\hbar^2 {}_{Pf}\Sigma_{mn}\mu_{gn}{}^{i}\mu_{nm}{}^{j}\mu_{mg}{}^{k}[(\omega_{ng} - \omega_3)(\omega_{mg} - \omega_2)]^{-1} \quad (1)$$

and

$$\beta_{vect} = \Sigma\mu_i\beta_i/|\mu|, \quad \beta_i = \beta_{iii} + 1/3\Sigma(\beta_{ijj} + \beta_{jij} + \beta_{jji}), \quad i, j = x, y, z \text{ and } i \neq j$$

where $\omega_3 = -\omega_1 - \omega_2$, and $\hbar\omega_{ng}$ or $\hbar\omega_{mg}$ is the transition energy from ground to excited states. In eq 1, μ's are the transition moment matrix elements which can be expressed as a sum of one-electron integrals, and when m = n the $\mu_{nn}{}^{i} = \mu_n{}^{i} - \mu_g{}^{i}$. The P_f is a full permutation operator by which the Cartesian indices are to be permuted along with the over input and output frequencies. The SOS perturbation theory expressions for the hyperpolarizability indicate that one requires dipole moments of ground state and excited states, and the transition moments from ground to excited states and from excited to excited states. These moments are obtained from the TDB3LYP calculations. The SOS expansion is, in general, infinite since the applied optical field mixes the molecular ground state with many excited states. For the calculation of β, we generally truncate the infinite SOS expansion to a finite one after apparent convergence of β has been reached. The SOS//TDB3LYP method is employed to calculate the hyperpolarizability β because it has a chemically intuitive simplicity and offers several advantages. First, it can identify specific virtual excitation processes among the eigenstates of the system that make the most significant contributions to β. In contrast, if the finite field (FF) technique is employed in the calculations of β, we yield only a final value of β with no information regarding its origin. The second advantage is that the dispersion character of β can be easily computed, whereas the FF method needs to solve repeatedly coupled Hamiltonian procedures with a different applied field. The third advantage is the capability to include the many-electron nature of the molecular wave functions at ground and excited states.

The geometries of monomer, dimers, and trimer of MNA molecules taken from experimental determination are used in all the calculations. As shown by X-ray crystallographic structural determination,[19] the MNA crystal belongs to the space group *Ia* with unit-cell parameters $a = 7.6113(5)$ Å, $b = 11.6304(7)$ Å, $c = 8.2286(5)$ Å, and $\beta = 94.050(2)°$. One unit-cell contains four MNA molecules, and they are grouped into two typical molecular pairs (two typical dimers). The configurations of the monomer, p- and h-dimers, and trimer of MNA molecules are shown in Figure 2. The molecular positions in the unit cell are determined from the crystallographic data[19] and the molecules are rotated to a standard orientation defined in the Gaussian 98 program[14] in the calculations.

3. Results and Discussion

3.1 Supermolecular Interactions. There are two typical dimers in MNA crystal reported from the X-ray crystallographic structure,[19] one for π-stacking dimer and the other one for hydrogen-bonded dimer. Hereafter, we call them the p-dimer and h-dimer of MNA supermolecules, respectively. The trimers within a MNA crystal are constructed from the h- and p-stacking configurations. To discuss intermolecular interactions in the dimer and trimer, we define a supermolecular interaction energy by the differences between the SCF energy of dimer and trimer (supermolecule) and the 2× and 3× SCF energies of monomer molecule, described as $E_{si} = E_{sup} - nE_{mono}$ ($n = 2, 3$). Here, the supermolecular interaction energies of E_{si} are contributions from all the types of intermolecular interaction energies within the B3LYP model, such as charge-transfer, electron correlation and exchange, and electrostatic interaction energies. Table 1 lists the SCF energies, charge distributions, and dipole moments of the monomer, p- and h-dimers, and trimer of MNA. It is found that the calculated E_{si} ($|-0.010301|$ au) of p-dimer is much larger than that ($|-0.003157|$ au) of h-dimer, and the E_{si} ($|-0.014189|$ au) of trimer is larger than that of both dimers in a MNA crystal. It is also found for the large charge transfers between the two C_6H_3 rings and a large HOMO−LUMO gap in the p-dimer of MNA crystal. This case tells us that there is a larger supermolecular interaction in the p-dimer than the h-dimer within MNA crystal. Figure 3 shows the frontier molecular orbitals of the monomer, two dimers, and trimer of MNA molecules, respectively. The highest occupied molecular orbital (HOMO) and lowest unoccupied molecular orbital (LUMO) are mostly contributions from the π-orbital characters of C_6H_3 ring and NH_2 group for monomer MNA molecule. The HOMO and LUMO of the p-dimer MNA supermolecule are the contributions from some mixings of MNA1 and MNA2 monomer molecules, and those of h-dimer MNA supermolecule are only contribution from MNA monomer molecule. The HOMO-2 orbital of the p-dimer MNA supermolecule is the contribution from a large mixing of MNA1 and MNA2 monomer molecules, and this evidence well shows that the charge transfers take place between the monomer MNA molecules for p-dimer. However, the HOMO-2 orbital of the h-dimer MNA supermolecule is only contribution from MNA monomer molecule, and this represents the interaction between the MNA molecules through hydrogen bond. It is also seen intuitively from Figure 2 that the interaction between the

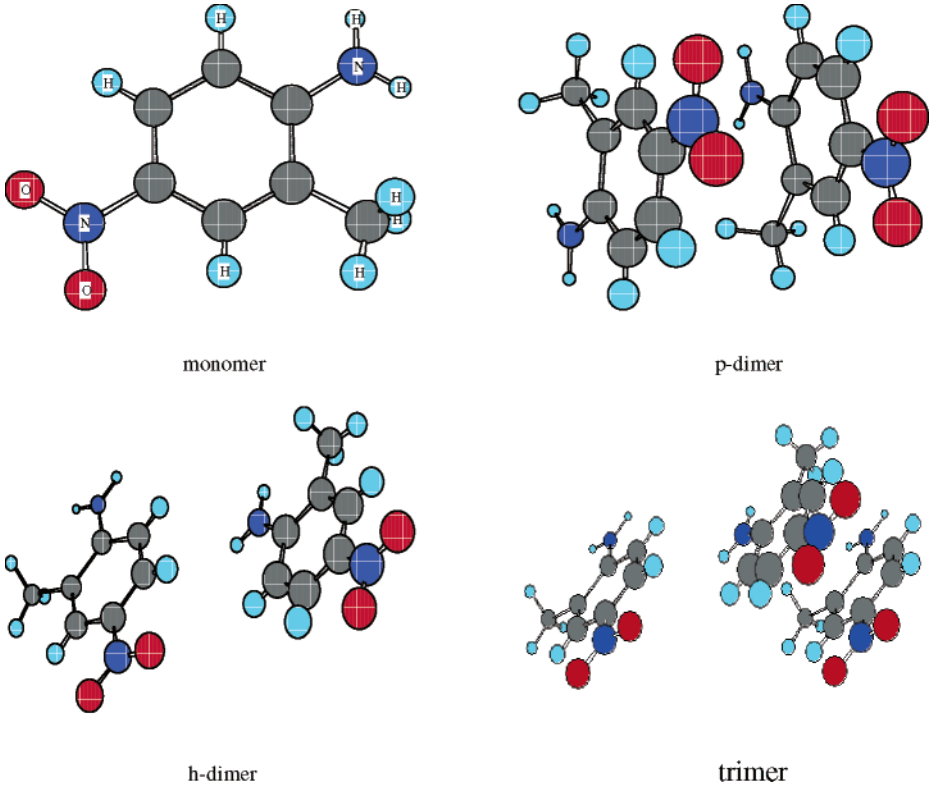

Figure 2. Configurations of the monomer, two typical dimers, and trimer MNA molecules.

TABLE 1: Calculated Properties of Monomer, Dimer, and Trimer MNA Molecules

property	monomer	p-dimer	h-dimer	trimer
E_{SCF} (au)	−528.407516399	−1056.82533315	−1056.81818978	−1585.23673704
E_{LU-HO} (au)	0.14806	0.14134	0.13416	0.13005
charge[a]	$A^{1.064-}B^{0.044-}C^{0.316-}D^{1.424+}$	$\begin{Bmatrix} A^{0.717+} & B^{0.542-} & C^{1.038-} & D^{0.876+} \\ A'^{0.250-} & B'^{0.441-} & C'^{0.582-} & D'^{1.260+} \end{Bmatrix}$	$\begin{Bmatrix} A^{1.025-} & B^{0.018-} & C^{0.393-} & D^{1.603+} \\ A'^{1.094-} & B'^{0.066-} & C'^{0.322-} & D'^{1.495+} \end{Bmatrix}$	
dipole (debye)	8.7436	15.5205	16.4885	23.2620

[a] A, A′ = C_6H_3; B, B′ = NH_2; C, C′ = NO_2; D, D′ = CH_3.

monomer MNA molecules for the h-dimer takes place lateral-wise whereas it is plane−plane (stack-wise) in the p-dimer configuration. Accordingly, the symmetry of the h-dimer arrangement is lower than that of the p-dimer one, and it has a larger dipole moment, as listed in Table 1. The frontier orbitals of the trimer are made up of both the p- and h-dimer frontier orbitals. It is indicated from the above analyses that the different dipole moments and supermolecular interactions between the h- and p-dimers originate from site effect, and those between the dimer and trimer originate from size effect among the MNA molecules.

3.2 Electronic Absorption Spectra. The calculated TDB3LYP absorption spectra for p- and h-dimers as well as trimer of MNA molecules are shown in Figure 4. For comparison, we also include in Figure 4 the spectra of monomer MNA molecule. It is found that the spectral shape is broad for monomer, and sharp for dimers and trimer. In all of the considered species, the spectral peak positions have no distinct changes and the lowest electronic transition absorption peaks are localized at about 4.0 eV. The absorption peaks result principally in electronic transition from the ground singlet state S_0 to the excited singlet states S_n ($n = 2$ for monomer, $n = 6$ for p-dimer, $n = 5$ for h-dimer, and $n = 10$ for trimer). State S_2 of monomer has most contribution from the configuration of $0.5780(\Psi_{40\rightarrow41})$ and the oscillator strength of the corresponding transition from ground state is 0.42. State S_6 of p-dimer has the greatest contributions from the configurations of $0.3476(\Psi_{79\rightarrow82}) - 0.3072(\Psi_{79\rightarrow81}) + 0.3662(\Psi_{80\rightarrow82})$, and the oscillator strength of the corresponding transition is 0.054. State S_5 of the h-dimer has the greatest contributions from the configurations of $0.4469(\Psi_{80\rightarrow82}) - 0.3653(\Psi_{79\rightarrow81})$, and the oscillator strength is 0.073. State S_{10} of trimer has the main contributions from the configurations of $-0.2826(\Psi_{119\rightarrow122}) + 0.3867(\Psi_{119\rightarrow123}) - 0.3457(\Psi_{120\rightarrow123})$, and the oscillator strength of the corresponding transition is 0.063. The calculated oscillator strengths show that the electronic absorption strength of h-dimer is largest among the studied species. As with the above statement about the orbital components of the HOMO and LUMO, we can infer that the lowest absorption peaks originate from the $\pi-\pi^*$ charge transfers within one MNA molecule for both the monomer and h-dimer, and between the two MNA molecules for the p-dimer. The calculated first transition energy corresponding to UV absorption edge is 3.6269, 3.1971, 3.1797, and 3.0697 eV, for the monomer, p-dimer, h-dimer, and trimer, in turn. The first transition energy of trimer is closer to the observed UV absorption edge of 2.689 eV (450 nm) of the MNA crstal.[8]

3.3 Second-Order Polarizabilities. For the calculations of β, we first consider how to truncate the infinite SOS expansion to a finite one. Figure 5 shows the plots of the calculated second-order polarizabilities $\beta_{tot}(-2\omega;\omega,\omega)$ at the TDB3LYP/3-21G+

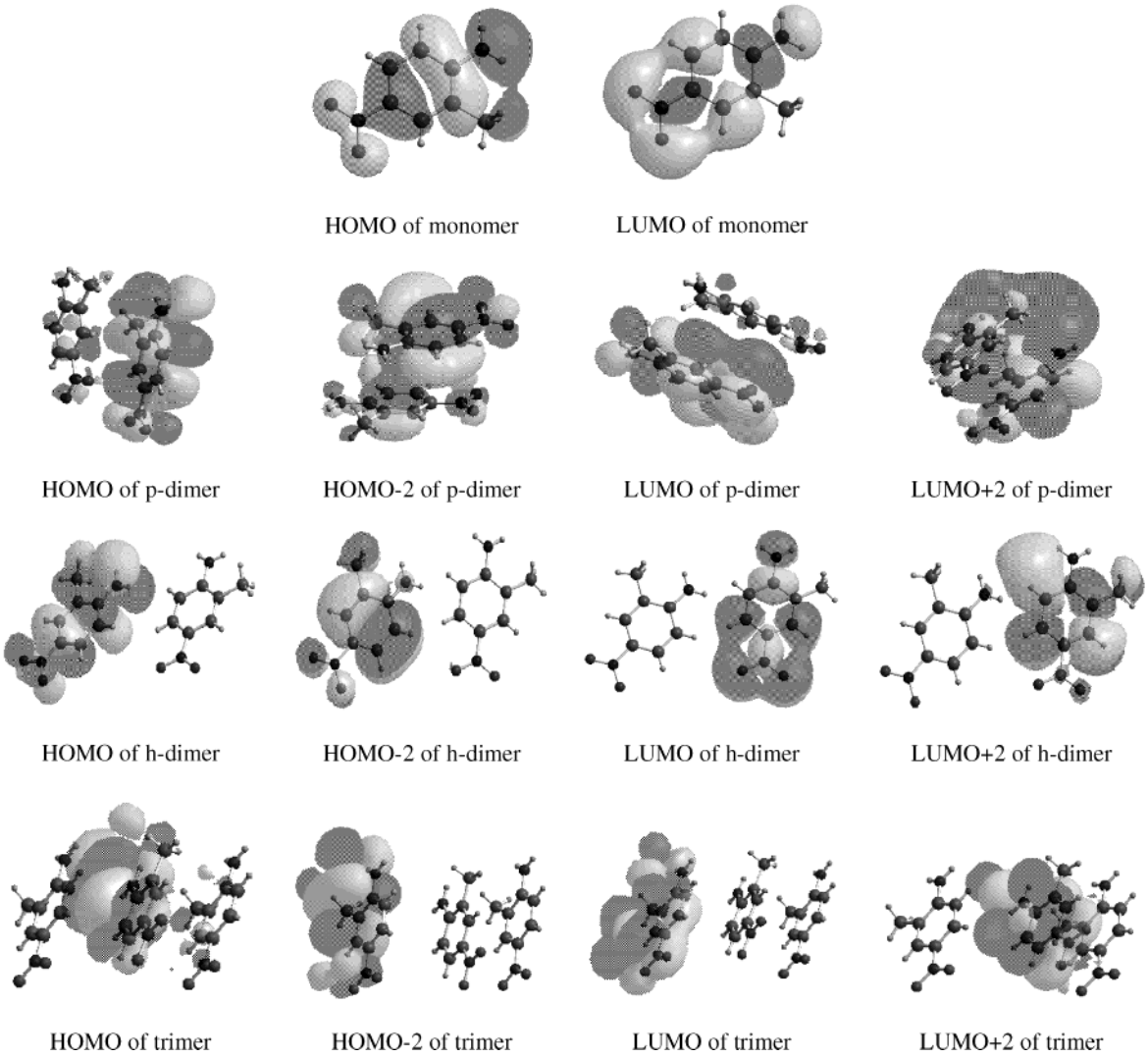

Figure 3. Frontier molecular orbitals of the monomer, two dimers, and trimer MNA molecules.

level vs. the number of states for the studied species at input photon energy of $\hbar\omega = 1.164$ eV. It is found that the curves have a similar shape; that is, a similar convergent behavior of β_{tot} in monomer, dimers, and trimer MNA supermolecules. These curves can be divided into two segments. The first segment formed below state 12 is a sharp variation, and the second segment formed after state 13 is smooth. For example, the calculated value of the β_{tot} including 11 states is separately about 48, 56, 77, and 85% of the β_{tot} value including 60 states at TDB3LYP/3-21G+ level for the monomer, p-dimer, h-dimer, and trimer MNA molecules. The calculated β_{tot} value obtained from summation over 48 states from the 12th state to the 60th state is about 52, 44, 23, and 15% of the β_{tot} value obtained from summation over 60 states for the monomer, p-dimer, h-dimer, and trimer MNA molecules, respectively. The convergent rate of the trimer is the fastest for the studied species, however, convergence is reached after summation over about 50 states for all of the studied species. This shows that it is reasonable in the calculations of β of the MNA supermolecules when we truncate 60 states by using the SOS//TDB3LYP methods.

The calculated frequency dependence of β_{tot} values is plotted in Figure 6 for the monomer, dimers, and trimer MNA molecules. It is found that the resonant enhancements appear after input energy larger than 1.3 eV, and no dispersion exists at input photon energy less than 1.1 eV for all the considered species. The β_{tot} values given above are found to be dominated by some excited charge-transfer states. For example, the 12th state of the monomer MNA has contributions of 90% to the β_{tot}, and this state has the greatest components from the configuration of $0.6327(\psi_{35\rightarrow41})$. The 5th state and 7th state of the p-dimer MNA have separate contributions of 21 and 16% to the β_{tot}, and these two states have the greatest components from the configurations of $0.5469(\psi_{79\rightarrow82}) - 0.3873(\psi_{80\rightarrow82})$ and $0.1012(\psi_{75\rightarrow81}) + 0.6779(\psi_{78\rightarrow81})$, respectively. The 5th state of the h-dimer MNA has contributions of 46% to the β_{tot}, and the state has the greatest components from the configurations of $0.4469(\psi_{80\rightarrow82}) - 0.3653(\psi_{79\rightarrow81})$. The 10th state of the trimer MNA has contributions of 55% to the β_{tot} and has the greatest contributions from the configurations of $-0.2826(\Psi_{119\rightarrow122}) + 0.3867(\Psi_{119\rightarrow123}) - 0.3457(\Psi_{120\rightarrow123})$. For the p-dimer MNA supermolecule, the configuration of $\psi_{79\rightarrow82}$ is constructed by one electron promotion from the HOMO $-$ 1 orbital (φ_{79}) to the LUMO + 1 (φ_{82}), and the configuration of $\psi_{78\rightarrow81}$ is constructed by one electron promotion from the HOMO -2 (φ_{78}) to the LUMO orbital (φ_{81}). The calculated electronic structures show that these molecular orbitals are made up from the mixing of the two monomer MNA molecular orbitals, as shown in Figure 3b. Therefore, it is clear that the charge transfers of intermolecules make considerate contributions to the first hyperpolarizability of p-dimer supermolecule. For the h-dimer MNA supermolecule, the molecular orbitals, φ_{79}, φ_{80}, φ_{81}, and

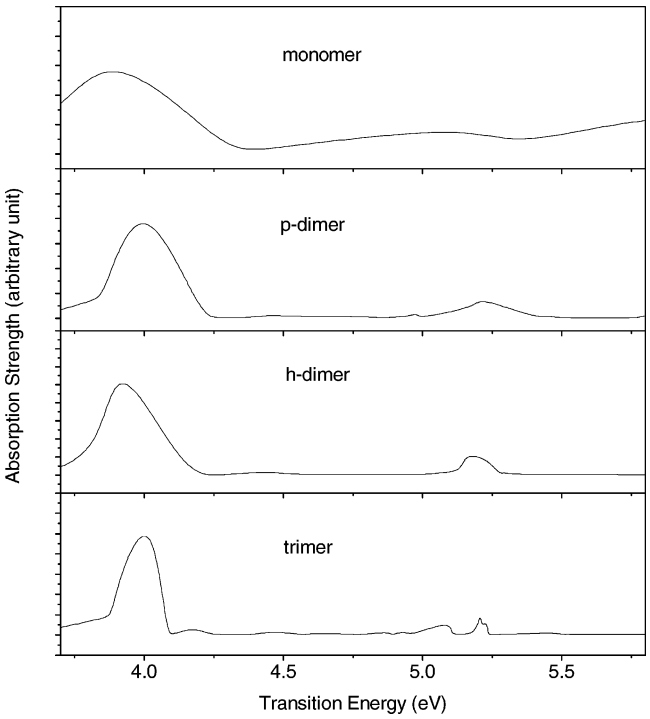

Figure 4. Calculated absorption spectra of monomer, dimer, and trimer MNA molecules based on TDB3LYP/3-21G+ level.

φ_{82} contributing to the configurations of $\psi_{80\rightarrow82}$ and $\psi_{79\rightarrow81}$, are constructed by only one monomer molecular orbital. This case indicates that the hydrogen-bonded interactions of intermolecules make significant contributions to the first hyperpolarizability of h-dimer supermolecule. Why is there a large hyperpolarizability for the h-dimer of MNA supermolecule? We can find evidences from the transition energies and moments of some important states contributing to hyperpolarizability. For example, at state 5 the transition moment (2.311 au) of the h-dimer is larger than that (0.82 au) of p-dimer, and the transition energies between the two dimers (3.89, 3.85 eV) are almost the same. It is seen from eq 1 that the first hyperpolarizability is governed by the product of the transition moments and the transition energy. Accordingly, a larger first hyperpolarizability mostly arises from larger dipole transition moments, in fact, which arises from the state function and spatial configuration of the h-dimer MNA supermolecule. The finding shows that the h-dimer with lateral-wise configuration is more favorable than the p-dimer with stack-wise arrangement to NLO response. This situation indicates a site effect on NLO response. The trimer consists of p- and h-dimers, and dipole moment of ground state is larger for the trimer than dimer, as listed in Table 1. This is the reason the first hyperpolarizability is larger for the trimer than dimer, and it indicates a size effect on NLO response in MNA supermolecule.

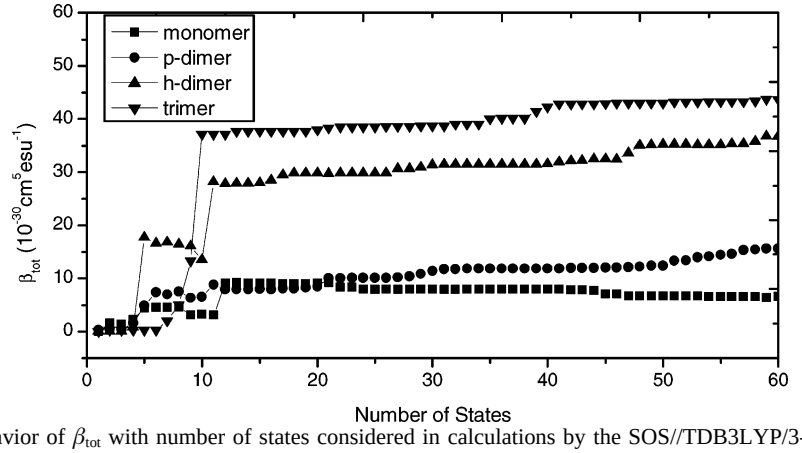

Figure 5. Convergence behavior of β_{tot} with number of states considered in calculations by the SOS//TDB3LYP/3-21G+ methods.

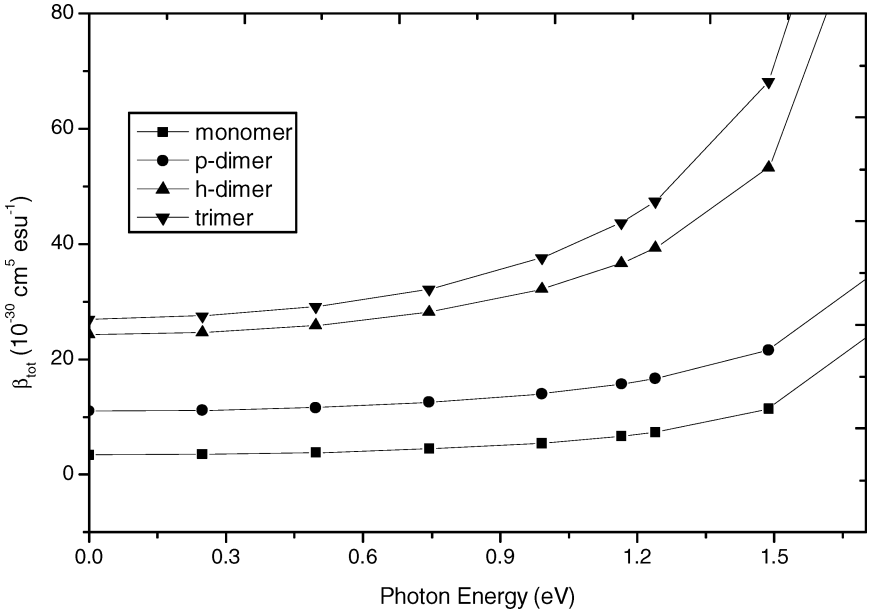

Figure 6. Frequency-dependent second-order polarizabilities of monomer, dimer, and trimer MNA molecules at the SOS//TDB3LYP/3-21G+ methods.

TABLE 2: Calculated β (10^{-30} cm^5 esu^{-1}) Components of Monomer, Dimer, and Trimer MNA Supermolecules at Input Wavelength of 1064 nm

component	monomer	p-dimer	h-dimer	trimer
x x x	−8.37	12.12	−13.17	−4.49
x y y	0.87	−0.09	−9.85	−12.81
y x y	1.87	0.46	−12.59	−13.50
x z z	0.19	2.46	−0.10	−0.67
z x z	0.22	2.27	−0.08	−1.07
y y y	−0.02	0.43	−15.22	28.27
y x x	−0.07	0.90	−12.01	7.11
x y x	−0.02	−0.01	−11.23	7.81
y z z	−0.03	2.04	−0.22	2.05
z y z	−0.04	2.21	−0.23	2.64
z z z	−0.05	0.30	0.02	0.98
z x x	−0.33	−6.62	0.11	1.93
x z x	−0.25	−5.72	0.17	2.21
z y y	0.00	1.46	−0.19	6.93
y z y	−0.02	1.04	−0.03	6.73
x y z	0.01	0.90	0.43	−3.09
y z x	−0.08	−0.15	0.54	−3.64
z x y	−0.04	0.68	0.44	−3.38
β_{tot}	6.64	14.55	36.64	43.74
β_{vec}	−6.58	15.67	36.70	43.73
$\|\|\beta\|\|$	8.53	17.97	33.62	41.99

3.4 Supermolecular Interactions Contributing to Crystal NLO Susceptibilities. To describe the influences of supermolecular interaction on hyperpolarizability, we can define a norm of the tensor of β hyperpolarizability,[20]

$$||\beta||^2 = \beta_{xxx}^2+\beta_{yyy}^2+\beta_{zzz}^2+3(\beta_{xyy}^2+\beta_{yxx}^2+\beta_{xzz}^2+\beta_{zxx}^2+\beta_{yzz}^2+\beta_{zyy}^2)+6\beta_{xyz}^2 \quad (2)$$

where the norm $||\beta||$ value is invariant to any rotation, that is, it is independent of orientation of molecular axis. Accordingly, the norm of the second-order susceptibility of MNA bulk crystal should have $||\chi|| = N_sL_s||\beta||_s = N_dL_d||\beta||_d = N_tL_t||\beta||_t$. Here, the superscripts s, d, and t symbolize monomer, dimer, and trimer of MNA molecules, respectively, the N and L are molecular density number and local field correction factor at radiation frequency ω. We note here that the molecular number density N is defined as the product of mass density and Avogadro's constant divided by the molar mass. So we have the relation of $N_s = 2N_d = 3N_t$, and $2L_s||\beta||_s = L_d^h||\beta||_d^h = L_d^p||\beta||_d^p$, and $3L_s||\beta||_s = L_t||\beta||_t$. The local field factor L describes an influence of the molecular environment and makes the enhancement of the molecular hyperpolarizabilities resulting from the mutual polarization effects among neighboring molecules in a crystal. We consider that the local field effects are different among the monomer MNA molecule, h-dimer, and p-dimer MNA supermolecules in a crystal because these selected molecules have different surrounding environments, and the local field factors have a relation of $L_d = I_{sper}L_s$. Accordingly, the first hyperpolarizabilities of monomer and dimer MNA molecules exist at a relationship of $2||\beta||_s = I_{sper}||\beta||_d$. The calculated components of β_{ijk} and the $||\beta||$ values are listed in Table 2 at an input photon energy of 1.165 eV. It is found that the 2× values of $||\beta||$ and β_{tot} of the monomer MNA molecule are quite near that of p-dimer MNA supermolecule. This means $I_{sper} \approx 1$ (local field factor $L_d^p \approx L_s$). The summation of individual monomer MNA molecular hyperpolarizability is equal to p-dimer MNA supermolecular hyperpolarizability, which means that the oriented-gas approximation works. This situation tell us that the $\pi-\pi^*$ charge transfers of intermolecules with stack-wise arrangement have no contributions to MNA crystal NLO susceptibilities. However, the $||\beta||$ and β_{tot} values of the h-dimer MNA supermolecule are above 100% larger than those estimated from the additivity of the monomer MNA $||\beta||$ values. These results are in agreement with that of Marks and coworkers calculated in a dimer of slipped configuration.[10] Recently, hydrogen bond effects on hyperpolarizability on urea molecular cluster have been reinvestigated and reported.[21] It is also found from Table 2 that the $||\beta||$ or β_{tot} value of trimer is about the same as the summations of $||\beta||$ or β_{tot} values of h-dimer and monomer. The obtained results are consistent with the arrangement of trimer constructed from both the lateral-wise and the stack-wise configurations.

TABLE 3: Calculated MNA Crystal Second-Order Susceptibilities from Different MNA Polymers

species	$\|\|\beta\|\|$ (10^{-30} cm^5 esu^{-1})	L	N (10^{21} mol/cm^3)	$\|\|\chi\|\|$ (10^{-7} esu)
monomer	8.53	8.0	5.50	3.76
p-dimer	17.97	8.0	2.75	3.95
h-dimer	33.62	8.0	2.75	7.40
trimer	41.99	8.0	1.83	6.15
experment				9.06

Now we make comparisons between the theoretical and experimental values. According to the same treatment as the norm $||\beta||$ in eq 2, we can obtain $||\chi||_{obs}$ to be 9.06×10^{-7} esu from the experimental values of $d_{11}(1.84 \times 10^{-10}$ m/V $= 4.39 \times 10^{-7}$ esu, $\chi = 2d$) and d_{12} (2.67×10^{-11} m/V $= 0.637 \times 10^{-7}$ esu, $\chi = 2d$).[22] Then we employ the relation of $||\chi|| = ||\beta||(NL)$. The N value of MNA crystal can be calculated from the mass density[19] and formula mass of monomer, dimer, and trimer MNA molecules. The local field correction factor is calculated from the $L = f_{2\omega}f_\omega^2$, and $f_\omega = [n_\omega^2 + 2]/3$ with the assumption of Lorentz−Lorenz local field,[23] in which the n_ω is refractive index of a crystal. Here we make an approximation of $n_\omega \approx n_{2\omega}$ and take $n_\omega = 2.0$ [2] in the calculations of L factor. Table 3 lists the parameters $||\beta||$, L, and N of calculating crystal susceptibility from the different polymers of MNA molecules, and experimental value of $||\chi||$. It is found that the calculated susceptibilities using the parameters of h-dimer and trimer are close to the experimental values of 9.06×10^{-7} esu, assuming the same local field correction for all of the studied species. For example, we use the N of 2.7527×10^{21} molecule/cm^3, L of 8.0, and the $||\beta||_{cal}$ value of 33.62×10^{-30} cm^5 esu^{-1} for h-dimer MNA supermolecule to obtain $||\chi||_{obs}$ of 7.40×10^{-7} esu. Accordingly, we can conclude that the supermolecular interactions through hydrogen bond with the slipped cofacial arrangements are more favorable to MNA crystal NLO response. However, a larger supermolecular interaction through charge transfers between the molecules with stack-wise arrangement will be small NLO response. These conclusions give a clue to design large NLO response crystal materials employing chromophoric arrangements with slipped configuration.

4. Summary

In this work, we first calculated the molecular orbitals and molecular interaction energies based on the B3LYP/3-21G+ level. Then we employed the time-dependent B3LYP method to compute the excited state properties and electronic absorption spectra. Finally, we used the SOS method to calculate the dynamic first hyperpolarizabilities of 2-methyl-4-nitroaniline monomer and its π-stacking and hydrogen-bonded dimers, as well as trimer constructed by π-stacking and slipped cofacial arrangements. To our knowledge, the SOS//TDDFT scheme is used to calculate nonlinear optical properties generally absent from the literature. The calculated results show that the hydrogen-bonded dimer has a smaller supermolecular interac-

tion, larger transition dipole moments, and second-order nonlinear optical response compared with that of the π-stacking dimer, and these results come from the site effect of dimer within MNA crystal. The lowest absorption peak originates from the $\pi-\pi^*$ charge transfers within a MNA molecule for hydrogen-bonded dimer, and between the two MNA molecules for the π-stacking dimer in a MNA crystal. A large value of $||\beta||$ of trimer originates from the size effect on nonlinear response. The resonant enhancement of hyperpolarizability appears after input energy larger than 1.3 eV, and no dispersion exists at input photon energy less than 1.1 eV for all the considered species. The hydrogen-bonded interactions of intermolecule have strong enhancements for the linear absorption and nonlinear optical response in the slipped cofacial arrangements of dimer in a MNA crystal. The reason the hydrogen-bonded dimer has a larger first hyperpolarizability mostly arises from larger dipole transition moments, which, in fact, arise from the state function and spatial configuration of the h-dimer MNA supermolecule. The obtained results will give a clue to design of new nonlinear optical materials employing nonlinear chromophoric arrangements in a crystal.

Acknowledgment. This investigation was based on work supported by the National Natural Science Foundation of China under projects 20373073 and 90201015, the Science Foundation of the Fujian Province (E0210028 and 2002F010), and the Foundation of State Key Laboratory of Structural Chemistry (030060).

References and Notes

(1) Lipscomb, G. F.; Garito, A. F.; Narang, R. S. *J. Chem. Phys*. **1981**, *75*, 1509.

(2) Levine, B. F.; Bethea, C. G.; Thurmond, C. D.; Lynch, R. T.; Bernstern, J. L. *J. Appl. Phys.* **1979**, *50*, 2523.

(3) White, J. D.; Hulin, D.; Joffre, M.; Migus, A.; Antonetti, A.; Toussaere, E.; Hierle, R.; Zyss, J. *Appl. Phys. Lett*. **1995**, *64*, 264.

(4) Xu, J.; Zhou, L.; Thakur, M. *Appl. Phys. Lett*. **1998**, *72*, 153.

(5) Gauvin, S.; Zyss, J. *J. Cryst. Growth* **1995**, *166*, 507.

(6) Damman, P.; Vallee, R.; Dosiere, M.; Toussaere, E.; Zyss, J. *Synth. Met.* **2001**, *124*, 227.

(7) Vallee, R.; Damman, P.; Dosiere, M.; Toussaere, E.; Zyss, J. *J. Am. Chem. Soc.* **2000**, *122*, 6701.

(8) Choi, J.; Aggarwal, M. D.; Wang, W. S. *J. Korean Phys. Soc*. **1998**, *32*, S1234.

(9) Goeta, A. E.; Wilson, C. C.; Autino, J. C.; Ellena, J.; Punte, G. *Chem. Mater.* **2000**, *12*, 3342.

(10) Bella, S. D.; Ratner, M. A.; Marks, T. J. *J. Am. Chem. Soc*. **1992**, *114*, 5842.

(11) Casida, M. E.; Jamorski, C.; Casida, K. C.; Salahub, D. R. *J. Chem. Phys.* **1988**, *180*, 4439.

(12) Bauernschmitt, R.; Ahlrichs, R. *Chem. Phys. Lett*. **1996**, *256*, 454.

(13) Stratman, R. E.; Scuseria, G. E.; Frisch, M. J. *J. Chem. Phys.* **1998**, *109*, 8218.

(14) Frisch, M. J.; Trucks, G. W.; Schlegel, H. B.; Scuseria, G. E.; Robb, M. A.; Cheeseman, J. R.; Zakrzewski, V. G.; Montgomery, J. A., Jr.; Stratmann, R. E.; Burant, J. C.; Dapprich, S.; Millam, J. M.; Daniels, A. D.; Kudin, K. N.; Strain, M. C.; Farkas, O.; Tomasi, J.; Barone, V.; Cossi, M.; Cammi, R.; Mennucci, B.; Pomelli, C.; Adamo, C.; Clifford, S.; Ochterski, J.; Petersson, G. A.; Ayala, P. Y.; Cui, Q.; Morokuma, K.; Malick, D. K.; Rabuck, A. D.; Raghavachari, K.; Foresman, J. B.; Cioslowski, J.; Ortiz, J. V.; Stefanov, B. B.; Liu, G.; Liashenko, A.; Piskorz, P.; Komaromi, I.; Gomperts, R.; Martin, R. L.; Fox, D. J.; Keith, T.; Al-Laham, M. A.; Peng, C. Y.; Nanayakkara, A.; Gonzalez, C.; Challacombe, M.; Gill, P. M. W.; Johnson, B. G.; Chen, W.; Wong, M. W.; Andres, J. L.; Head-Gordon, M.; Replogle, E. S.; Pople, J. A. Gaussian 98; Gaussian, Inc.: Pittsburgh, PA, 1998.

(15) Gross, E. K. U.; Kohn, W. *Adv. Quantum Chem.* **1990**, *21*, 255.

(16) Runge, E.; Gross, E. K. U. *Phys. Rev. Lett*. **1984**, *52*, 977.

(17) Ward, J. F. *Rev. Mod. Phys*. **1965**, *37*, 1.

(18) Orr, B. J.; Ward, J. F. *Mol. Phys*. **1971**, *20*, 513.

(19) Ferguson, G.; Glidewell, C.; Low, J. N.; Skakle, M. S.; Wardell, J. L.; *Acta Crystallogr*. **2001**, *C57*, 315.

(20) Zyss, J. In *Nonlinear Optics*; Miyata, S., Ed.; Elsevier Science: Amsterdam, 1992; p 33.

(21) Wu, K.; Snijders, J. G.; Lin, S. *J. Phys. Chem. B* **2002**, *106*, 8954.

(22) Zhang, K.-C.; Wang, X.-M. *Nonlinear Optical Crystal Material Sciences*; Kexue Publishers: Beijing, 1996; p 302.

(23) Boy, R. W. *Nonlinear Optics*; Academic Press: San Diego, CA, 1992; p 148.